Drug Delivery

DOI: 10.1002/ange.201307247

Efficacious Anticancer Drug Delivery Mediated by a pH-Sensitive Self-Assembly of a Conserved Tripeptide Derived from Tyrosine Kinase NGF Receptor**

*Parikshit Moitra, Krishan Kumar, Paturu Kondaiah, and Santanu Bhattacharya**

Abstract: *We present herein a short tripeptide sequence (Lys–Phe–Gly or KFG) that is situated in the juxtamembrane region of the tyrosine kinase nerve growth factor (Trk NGF) receptors. KFG self-assembles in water and shows a reversible and concentration-dependent switching of nanostructures from nanospheres (vesicles) to nanotubes, as evidenced by dynamic light scattering, transmission electron microscopy, and atomic force microscopy. The morphology change was associated with a transition in the secondary structure. The tripeptide vesicles have inner aqueous compartments and are stable at pH 7.4 but rupture rapidly at pH ≈ 6. The pH-sensitive response of the vesicles was exploited for the delivery of a chemotherapeutic anticancer drug, doxorubicin, which resulted in enhanced cytotoxicity for both drug-sensitive and drug-resistant cells. Efficient intracellular release of the drug was confirmed by fluorescence-activated cell sorting analysis, fluorescence microscopy, and confocal microscopy.*

The design and development of different nanobiomaterials mimicking natural processes is among the leading approaches in nanobiotechnology.[1] Toward therapeutic goals, one of the emerging interests is the development of biocompatible nanocarriers for efficient drug delivery.[2] The main aim is to overcome barriers that stand against the therapeutic potential of drugs, like overload side-effects,[3] specific cell targeting,[4] the development of multidrug resistance (MDR),[5] and the blood–brain barrier in gliomas.[6] In order to solve such outstanding problems, "decorated" liposomes,[7] multifunctional micelles,[8] polymeric hydrogels,[9] functionalized organic[10] and inorganic nanomaterials,[11] etc. have been employed. Among these, building blocks that are organized from short peptide sequences have become promising tools for biomedical applications.[12,13]

Recently, stimuli-responsive morphological transformations of short peptide sequences in water have also been reported.[12,14] We considered a short tripeptide sequence (Lys–Phe–Gly or KFG) that is situated in the juxtamembrane region of the tyrosine kinase nerve growth factor (Trk NGF) receptors, which are involved in neuronal growth and differentiation. The absence of the KFG sequence in the receptor polypeptide chain seriously affects the activation of signaling cascades including the Ras superfamily, phosphoinositide 3-kinase, and the Suc1-associated neurotrophic factor target (SNT) protein.[15] This also results in impaired neurite outgrowth and sometic hypertrophy. This small but critically conserved entity, which plays an important role in the growth factor signal transduction process, was chosen for the present study. We investigated this biologically important tripeptide, KFG (Figure 1), which spontaneously self-assembled into

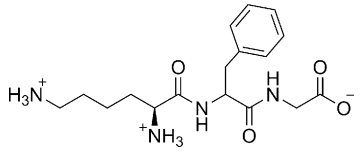

Figure 1. Molecular structure of the synthesized tripeptide, KFG.

defined nanostructures in aqueous media. The tripeptide showed an exciting phenomenon of reversible and concentration-dependent switching of nanostructures between nanovesicles and nanotubes. This change in morphology was associated with a transition in the secondary structure at the peptide level. The vesicles that resulted from the self-assembly of KFG were extremely sensitive toward the pH value of the medium. They were stable at pH 7.4 but ruptured rapidly at pH ≈ 6. This property is often exploited for improved cellular internalizations in anticancer drug delivery.[11c,16] The pH-sensitive nature of the vesicles was accordingly tested for the delivery of one of the most widely used drugs for many types of cancer, doxorubicin (DOX). Cellular uptake of DOX dramatically increased after the drug was loaded into the vesicles. Overall, we report for the first time a smart stimulus-responsive (pH-induced) tripeptide-based self-assembled nanocarrier that induces significant therapeutic delivery of a chemotherapeutic drug, DOX, to cancer cells.

To discern the nature of the supramolecular structures that were formed upon self-assembly of Lys–Phe–Gly, dynamic light scattering (DLS) measurements were performed. At a low concentration of the tripeptide (0.5 mg mL^{-1}), nanostructures of approximately 50–70 nm

[*] P. Moitra,[+] K. Kumar,[+] Prof. S. Bhattacharya
Department of Organic Chemistry
Indian Institute of Science, Bangalore 560 012 (India)
E-mail: sb@orgchem.iisc.ernet.in
Prof. P. Kondaiah
Department of Molecular Reproduction, Development and Genetics
Indian Institute of Science, Bangalore 560 012 (India)
[+] These authors contributed equally to this work.

[**] NGF = Nerve growth factor. This work was supported by the J. C. Bose Fellowship grant of the Department of Science and Technology to S.B. Doxorubicin-resistant HeLa cells were a kind gift from Dr. Annapoorni Rangarajan. We thank the Chemical Sciences Division for the transmission electron microscopy facility.
Supporting information for this article is available on the WWW under http://dx.doi.org/10.1002/anie.201307247.

were observed, whereas aggregates of about 190–200 nm were formed at a higher concentration (5 mg mL^{-1}; Figure S5 in the Supporting Information). Interestingly, we found that this transition in the sizes of the nanostructures is reversible in nature (Figure S6). These observations prompted us to investigate the KFG aggregates at various concentrations by using transmission electron microscopy (TEM). The tripeptide formed spherical structures with diameters of (50 ± 10) nm at the low concentration, whereas it formed tubular aggregates with diameters of (190 ± 10) nm at the higher concentration (Figure S7). Atomic force microscopy (AFM; Figure 2) showed morphological features of the tripeptide aggregates similar to those observed in the TEM observations.

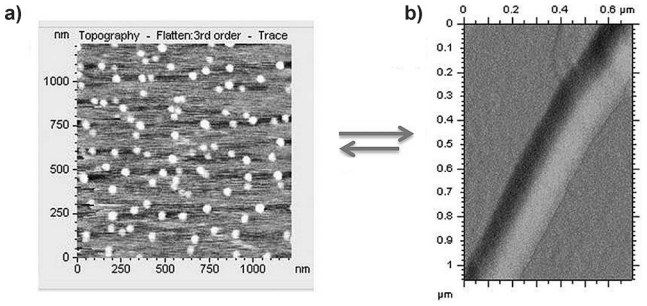

Figure 2. AFM images showing the topography of the KFG tripeptide at different concentrations: a) 0.5 mg mL^{-1} and b) 5 mg mL^{-1}. The double arrow between (a) and (b) indicates that the transition from nanovesicles to nanotubes is reversible as a function of concentration.

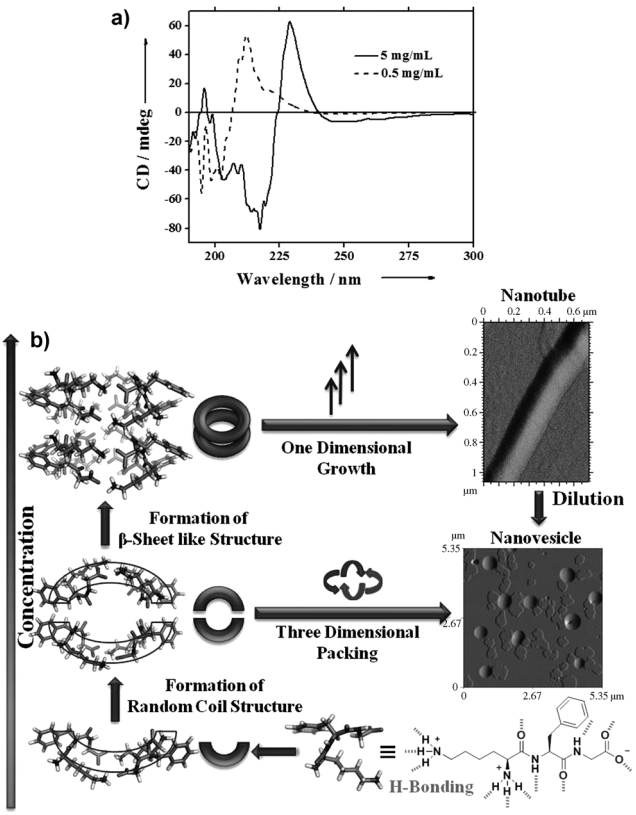

Figure 3. a) CD spectra of KFG at two different concentrations. b) Schematic illustration of the concentration-dependent self-assembly process of the tripeptide.

The thermotropic properties of the tripeptide self-assemblies at both concentrations in aqueous media were investigated by high-sensitivity differential scanning calorimetry (DSC).[17] The suspension of KFG at low concentration (vesicles) did not show any transition in the temperature range 20–70 °C, but at the higher concentration (nanotubes), the tripeptide showed a quasireversible transition during heating and cooling scans. Two peaks appeared at approximately 47 and 60 °C (Figure S8). The DSC results were corroborated by using temperature-dependent AFM studies at low and high concentrations (Figure S9). There was no change in the morphology of the vesicles even after the sample had been heated up to 85 °C, but the nanotubes changed topology upon heating. The transition from tubular to spherical nanostructures (vesicles) started occurring from 45 °C and ended at 60 °C. Above 90 °C, the vesicular structures collapsed, probably due to water evaporation. Interestingly, such a temperature-induced transition from tubular-to-vesicular morphology is quite unprecedented.

At higher concentration (5 mg mL^{-1}), the tripeptide exhibited a maximum at 196 nm and a minimum at 218 nm in the CD spectrum (Figure 3). This signature in the CD spectrum is analogous to those of β sheets in polypeptides. After dilution of this suspension to 0.5 mg mL^{-1}, the CD spectrum showed a negative band at 195 nm together with a positive band at 212 nm, which suggests the formation of a 'random-coil' structure.[18] This change in the secondary structure from a β sheet to a random coil occurs upon dilution of the tripeptide, which is also associated with the morphological transition. Again, such a reversible transition from vesicles to nanotubes along with changes in the secondary structure is rarely observed, to the best of our knowledge. Furthermore, we examined the self-assembly by molecular modeling studies (Figure S10), which evidenced that the peptide assemblies are formed mainly due to the interplay of electrostatic, π-stacking, and H-bonding interactions.

Even if the particles appear to be nearly spherical, it may not necessarily signify that they are vesicles and not solid nanoparticles. It is important to know whether the nanospheres derived from the tripeptide assemblies possess inner aqueous compartments. Therefore, we attempted to encapsulate a water-soluble solute or a drug in such particles. Toward this end, we employed a cationic dye, methylene blue (MB),[19] to check the entrapment capacities of the spherical aggregates in aqueous media. Indeed, the vesicles could encapsulate approximately 6.8 % of the total dye inside their inner aqueous compartments (Figure S11). In another experiment, we found that these tripeptide vesicles were also able to encapsulate the neutral, impermeant, water-soluble solute glucose[20] (Figure S12), which has no π-stacking unit, unlike the commonly available aromatic dyes.

Furthermore, because the tripeptide formed nanovesicles spontaneously at physiological pH values and the same vesicles could be disrupted at pH 6, we thought of exploiting this property for drug delivery.[16,21] Accordingly, we loaded

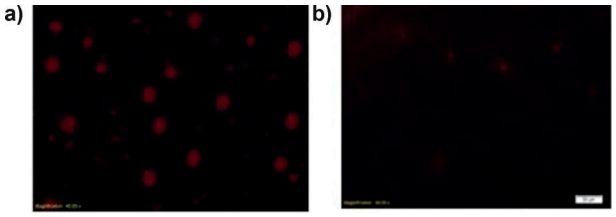

Figure 4. Fluorescence microscopy images of a) DOX-loaded vesicles at pH 7.4 and b) the disruption of the vesicles and drug release at pH 6. Scale bar: 20 μm.

the vesicles with DOX at pH 7.4 (Figure 4a) and followed the release of the drug at pH 6 upon rupture of the vesicles (Figure 4b). The percentage of DOX encapsulation was approximately 25.7%, and importantly, the resulting DOX-loaded vesicles were also quite stable in buffer containing serum (Figure S14). The kinetic profile obtained for the system showed a zero-order drug release at pH 6, which could be explained on the basis of a non-Fickian diffusion mechanism,[22] as fitted from the Peppas model (Figure S15). Also, the drug release profile of the DOX-loaded vesicles showed a bimodal release profile, with an initial burst release followed by a sustained release (Figure S14). A plausible reason for this burst release could be the disruption of the vesicular self-assembly and the increased hydrophilicity of DOX molecules at this lowered pH value. The remaining amount of DOX, which followed a sustained release profile thereafter, could be attributed to the partial adsorption effects between the tripeptide assembly and the DOX molecules, as reported in other nanocarrier systems.[11a]

The toxicity of the KFG nanovesicles was assayed in cell lines of different origins, namely HeLa (human cervical carcinoma), HEK 293T (human embryonic kidney, transformed), U251 (glioblastoma), and A549 (human lung adenocarcinoma) cells. The toxic effect of the empty vesicles appeared to be insignificant toward each cell line, with > 95% cells found to be viable (Figure 5a). The toxicity of the DOX-loaded vesicles was then assessed in the same set of cell lines and compared with that of free DOX. Notably, the cytotoxicity due to the DOX-loaded vesicles was significantly greater than that of free DOX at each of the examined concentrations (10, 20, 30, and 40 $\mu g\,mL^{-1}$) for the same period of incubation in all of the cells studied. The differences in cell viabilities between the treatment with DOX alone and the DOX-loaded vesicles at a representative 20 $\mu g\,mL^{-1}$ drug concentration in the above cells are shown in Figure 5b.

To explore the possible reasons for the enhanced toxicity, the internalization of DOX before and after being loaded into the KFG vesicles was examined, both by fluorescence-activated cell sorting (FACS) analysis and fluorescence microscopy. Based on the FACS data, the geometric mean of fluorescence intensity (GMFI) values for cells treated with DOX-loaded KFG vesicles were significantly higher than those of the free-DOX-treated cells. This effect was more prominent with increased exposure to and concentrations of DOX (Figure 6a) and remained consistent among all of the cell lines studied. Representative flow cytometry dot plots and histograms for DOX internalization are shown in Figure S16 and S17a, respectively. The fluorescence microscopy results substantiated the observation that the fluorescence intensity of the DOX was significantly higher for cells treated with DOX-loaded peptide vesicles than for the free-DOX-treated cells after 1 h of incubation (Figure S17). We also assessed the intracellular localization of the drug by confocal microscopy. Interestingly, cells treated with the DOX-loaded vesicles for 4 h showed nuclear localization of the drug with

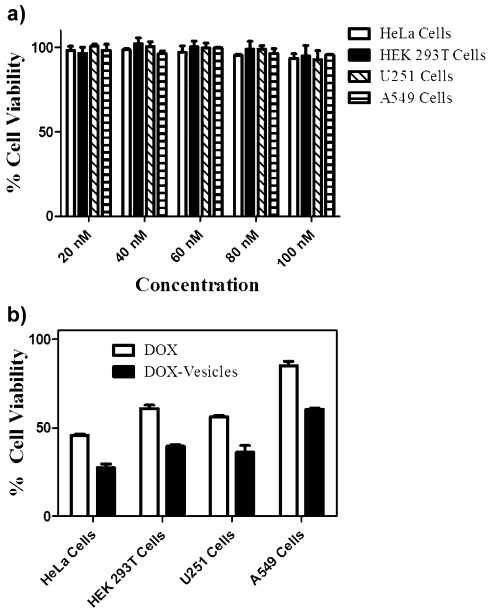

Figure 5. a) Cytotoxicity of the tripeptide vesicles at different concentrations. b) Cytotoxicity of DOX-loaded vesicles in comparison with free DOX at a concentration of 20 $\mu g\,mL^{-1}$.

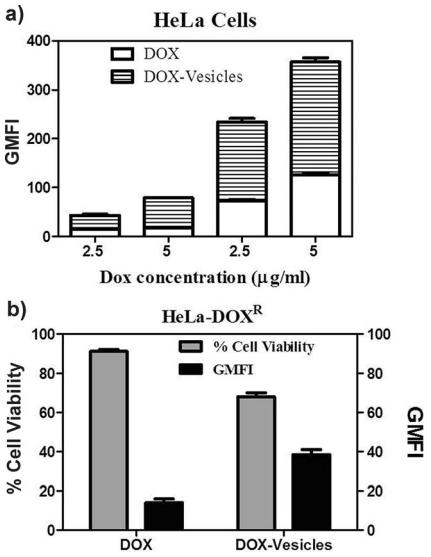

Figure 6. a) GMFI of DOX internalizations in HeLa cells at two different concentrations based on FACS analysis. The first two stacked bars show the results after 1 h and the second two stacked bars show the results after 4 h. b) Cytotoxicity of DOX-loaded vesicles in HeLa-DOX^R cells relative to the cytotoxicity with free DOX (20 $\mu g\,mL^{-1}$), and GMFI values in HeLa-DOX^R cells after a 4 h incubation (10 $\mu g\,mL^{-1}$).

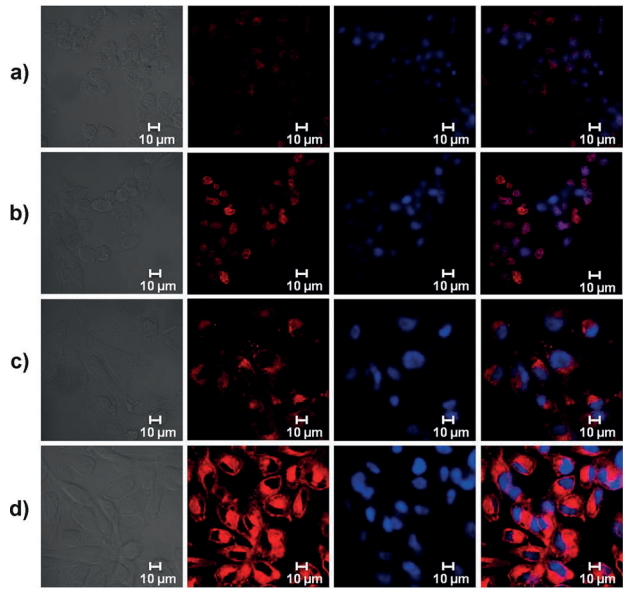

Figure 7. Representative confocal microscopy images after DOX treatment of HeLa cells at 5 $\mu g\,mL^{-1}$ for 4 h (a,b) and HeLa-DOX^R cells at 20 $\mu g\,mL^{-1}$ for 24 h (c,d). Panels (a) and (c) represent treatment with free DOX and panels b and d represent treatment with DOX-loaded vesicles. Each panel, from left to right, shows the bright-field image, DOX fluorescence (red), 4′,6-diamidino-2-phenylindole (DAPI) stained nuclei (blue), and an overlay of the last two.

much brighter DOX fluorescence than that observed in cells treated with DOX alone (Figure 7a,b). This observation was tested by quantifying the increase in fluorescence intensity of the internalized DOX by using confocal microscopic images of several independent experiments (Figure S19). Scatter diagrams (Figure S18) for the representative confocal microscopy images also substantiated the colocalization phenomenon. This observation is striking because the nuclear localization of drugs delivered by nanomaterials is known to be challenging.[23]

This interesting phenomenon of accelerated drug release and, thereby, increased cytotoxicity selectively toward the cancer cells encouraged us to deal with drug-resistant cell lines. We, therefore, performed cell viability experiments and drug internalization studies in DOX-resistant HeLa cells (HeLa-DOX^R). In this case also, the DOX-loaded vesicles were found to be more efficient in delivering a larger amount of the drug at fixed concentrations and time points, which imparted greater toxicity than the free DOX (Figure 6b). Confocal microscopy was performed for HeLa-DOX^R at relatively longer time points and higher drug concentrations because of the drug-efflux-related issues in drug-resistant cell lines. At an optimized concentration and time point, cells treated with DOX-loaded vesicles showed much higher DOX fluorescence than those treated with free DOX, although the drug was mainly localized in the cytoplasm this time (Figure 7c,d). Thus, the increased internalization of the drug could be attributed to the pH-sensitive response of the vesicles.

In summary, we have synthesized a natural tripeptide (KFG), which self-assembles to produce vesicles at lower concentration (0.5 $mg\,mL^{-1}$) and hollow nanotubes at higher concentration (5 $mg\,mL^{-1}$). The secondary structure of the tripeptide changes from random-coil to β-sheet-like assemblies as the concentration is increased. The transition scheme in the secondary structure is corroborated well with a molecular modeling study. The vesicles rupture and release their contents at $pH \approx 6$. A continuous drug release profile consistent with zero-order kinetics is maintained so that the concentration of drug remains constant throughout its delivery period. The pH-targeted drug delivery results in an enhanced cytotoxicity to both drug-sensitive and drug-resistant cells in vitro. The efficient intracellular release of the drug after loading into vesicles was confirmed by FACS analysis, fluorescence microscopy, and confocal microscopy. These tripeptide vesicles show the distinct advantage of pH-driven translocation even in serum, which may be important because it may bypass factors involved in drug resistance.

Such a system is therefore highly promising as a stimulus-responsive biocompatible nanovehicle that translocates into cells once exposed to the tumor pH regime. The fact that this tripeptide could be either synthesized readily or obtained commercially makes it particularly attractive for the delivery of anticancer drugs selectively to the cancer site with relevant functionalizations. We are now extending the utility of this by exploring its therapeutic potential toward other MDR cell lines with specific recognition sites in vivo. With the aim of eradicating the root of cancer, the specialized cancer stem cells that are responsible for the resistance to cancer therapies and the recurrence of cancer, work is underway to achieve targeting by a combination chemotherapeutic approach with the design of appropriate aptamer-loaded tripeptide nanocarriers.

Received: August 18, 2013
Revised: November 4, 2013
Published online: December 11, 2013

Keywords: drug delivery · nanostructures · peptides · pH sensitivity · self-assembly

[1] a) J. Lei, H. Ju, *Chem. Soc. Rev.* **2012**, *41*, 2122 – 2134; b) H. Robson Marsden, A. Kros, *Angew. Chem.* **2010**, *122*, 3050 – 3068; *Angew. Chem. Int. Ed.* **2010**, *49*, 2988 – 3005; c) C. Sanchez, H. Arribart, M. Madeleine, G. Guillie, *Nat. Mater.* **2005**, *4*, 277 – 288.

[2] a) N. Kamaly, Z. Xiao, P. M. Valencia, A. F. Radovic-Moreno, O. C. Farokhzad, *Chem. Soc. Rev.* **2012**, *41*, 2971 – 3010; b) S. K. Misra, P. Kondaiah, S. Bhattacharya, C. N. R. Rao, *Small* **2012**, *8*, 131 – 143; c) S. K. Misra, P. Moitra, B. S. Chhikara, P. Kondaiah, S. Bhattacharya, *J. Mater. Chem.* **2012**, *22*, 7985 – 7998.

[3] a) C. Cai, L. Lothstein, R. R. Morrison, P. A. Hofmann, *J. Pharmacol. Exp. Ther.* **2010**, *335*, 223 – 230; b) P. K. Singal, T. Li, D. Kumar, I. Danelisen, N. Iliskovic, *Mol. Cell. Biochem.* **2000**, *207*, 77 – 85.

[4] a) S. A. Mackowiak, A. Schmidt, V. Weiss, C. Argyo, C. V. Schirnding, T. Bein, C. Brauchle, *Nano Lett.* **2013**, *13*, 2576 – 2583; b) S. R. Paliwal, R. Paliwal, H. C. Pal, A. K. Saxena, P. R. Sharma, P. N. Gupta, G. P. Agrawal, S. P. Vyas, *Mol. Pharm.* **2012**, *9*, 176 – 186.

[5] a) J. Jiang, S. Yang, J. Wang, L. Yang, Z. Xu, T. Yang, X. Liu, Q. Zhang, *Eur. J. Pharm. Biopharm.* **2010**, *76*, 170 – 178; b) D. Peer,

J. M. Karp, S. Hong, O. C. Farokhzad, R. Margalit, R. Langer, *Nat. Nanotechnol.* **2007**, *2*, 751 – 760.
[6] a) H. Chen, Y. Qin, Q. Zhang, W. Jiang, L. Tang, J. Liu, Q. He, *Eur. J. Pharm. Sci.* **2011**, *44*, 164 – 173; b) W. Tian, X. Ying, J. Du, J. Guo, Y. Men, Y. Zhang, R. Li, H. Yao, J. Lou, L. Zhang, W. Lu, *Eur. J. Pharm. Sci.* **2010**, *41*, 232 – 243.
[7] a) B. Yang, S. Geng, X. Liu, J. Wang, Y. Chen, Y. Wang, J. Wang, *Soft Matter* **2012**, *8*, 518 – 525; b) S. H. Jung, S. H. Jung, H. Seong, S. H. Cho, K. Jeong, B. C. Shin, *Int. J. Pharm.* **2009**, *382*, 254 – 261.
[8] a) A. L. Z. Lee, S. H. K. Dhillon, Y. Wang, S. Pervaiz, W. Fan, Y. Y. Yang, *Mol. BioSyst.* **2011**, **7**, 1512 – 1522; b) T. Kim, C. W. Mount, W. R. Gombotz, S. H. Pun, *Biomaterials* **2010**, *31*, 7386 – 7397; c) J. P. K. Tan, S. H. Kim, F. Nederberg, K. Fukushima, D. J. Coady, A. Nelson, Y. Y. Yang, J. L. Hedrick, *Macromol. Rapid Commun.* **2010**, *31*, 1187 – 1192; d) S. Bhattacharya, S. K. Samanta, *J. Phys. Chem. Lett.* **2011**, *2*, 914 – 920.
[9] a) C. T. Huynh, M. K. Nguyen, J. H. Kim, S. W. Kang, B. S. Kim, D. S. Lee, *Soft Matter* **2011**, *7*, 4974 – 4982; b) D. P. Huynh, G. J. Im, S. Y. Chae, K. C. Lee, D. S. Lee, *J. Controlled Release* **2009**, *137*, 20 – 24.
[10] a) J. O. You, P. Guo, D. T. Auguste, *Angew. Chem.* **2013**, *125*, 4235 – 4240; *Angew. Chem. Int. Ed.* **2013**, *52*, 4141 – 4146; b) J. Liu, W. Bu, L. Pan, J. Shi, *Angew. Chem.* **2013**, *125*, 4471 – 4475; *Angew. Chem. Int. Ed.* **2013**, *52*, 4375 – 4379.
[11] a) Z. Y. Zhang, Y. D. Xu, Y. Y. Ma, L. L. Qiu, Y. Wang, J. L. Kong, H. M. Xiong, *Angew. Chem.* **2013**, *125*, 4221 – 4225; *Angew. Chem. Int. Ed.* **2013**, *52*, 4127 – 4131; b) Z. Zhao, D. Huang, Z. Yin, X. Chi, X. Wang, J. Gao, *J. Mater. Chem.* **2012**, *22*, 15717 – 15725; c) Z. Zhao, H. Meng, N. Wang, M. J. Donovan, T. Fu, M. You, Z. Chen, X. Zhang, W. Tan, *Angew. Chem.* **2013**, *125*, 7635 – 7639; *Angew. Chem. Int. Ed.* **2013**, *52*, 7487 – 7491.
[12] a) J. Naskar, S. Roy, A. Joardar, S. Das, A. Banerjee, *Org. Biomol. Chem.* **2011**, *9*, 6610 – 6615; b) X. Yan, Y. Cui, Q. He, K. Wang, J. Li, W. Mu, B. Wang, Z. Ou-yang, *Chem. Eur. J.* **2008**, *14*, 5974 – 5980; c) X. Yan, Q. He, K. Wang, L. Duan, Y. Cui, J. Li, *Angew. Chem.* **2007**, *119*, 2483 – 2486; *Angew. Chem. Int. Ed.* **2007**, *46*, 2431 – 2434.
[13] a) F. Zhao, M. Ma, B. Xu, *Chem. Soc. Rev.* **2009**, *38*, 883 – 891; b) M. Reches, E. Gazit, *Curr. Nanosci.* **2006**, *2*, 105 – 111; c) X. Gao, H. Matsui, *Adv. Mater.* **2005**, *17*, 2037 – 2050.
[14] a) D. Ke, C. Zhan, A. D. Q. Li, J. Yao, *Angew. Chem.* **2011**, *123*, 3799 – 3803; *Angew. Chem. Int. Ed.* **2011**, *50*, 3715 – 3719; b) T. Wang, J. Jiang, Y. Liu, Z. Li, M. Liu, *Langmuir* **2010**, *26*, 18694 – 18700; c) J. Naskar, A. Banerjee, *Chem. Asian J.* **2009**, *4*, 1817 – 1823; d) A. MaHam, Z. Tang, H. Wu, J. Wang, Y. Lin, *Small* **2009**, *5*, 1706 – 1721; e) T. Lu, F. Han, Z. Li, J. Huang, H. Fu, *Langmuir* **2006**, *22*, 2045 – 2049.
[15] a) X. Peng, L. A. Greene, D. R. Kaplan, R. M. Stephens, *Neuron* **1995**, *15*, 395 – 406; b) M. Ashcroft, R. M. Stephens, B. Hallberg, J. Downward, D. R. Kaplan, *Oncogene* **1999**, *18*, 4586 – 4597.
[16] a) Q. Duan, Y. Cao, Y. Li, X. Hu, T. Xiao, C. Lin, Y. Pan, L. Wang, *J. Am. Chem. Soc.* **2013**, *135*, 10542 – 10549; b) W. Gao, J. M. Chan, O. C. Farokhzad, *Mol. Pharm.* **2010**, *7*, 1913 – 1920; c) E. S. Lee, Z. Gao, Y. H. Bae, *J. Controlled Release* **2008**, *132*, 164 – 170.
[17] S. Bhattacharya, A. Srivastava, A. Pal, *Angew. Chem.* **2006**, *118*, 3000 – 3003; *Angew. Chem. Int. Ed.* **2006**, *45*, 2934 – 2937.
[18] N. E. Davis, L. S. Karfeld-Sulzer, S. Ding, A. E. Barron, *Biomacromolecules* **2009**, *10*, 1125 – 1134.
[19] a) S. Bhattacharya, J. Biswas, *Langmuir* **2011**, *27*, 1581 – 1591; b) S. Bhattacharya, Y. K. Ghosh, *Langmuir* **2001**, *17*, 2067 – 2075.
[20] R. M. Uda, T. Tanabe, Y. Nakahara, K. Kimura, *Soft Matter* **2008**, *4*, 560 – 563.
[21] a) M. Chanana, P. R. Gil, M. A. C. Duarte, L. M. L. Marzan, W. J. Parak, *Angew. Chem.* **2013**, *125*, 4273 – 4277; *Angew. Chem. Int. Ed.* **2013**, *52*, 4179 – 4183; b) M. A. Yassin, D. Appelhans, R. G. Mendes, M. H. Rummeli, B. Voit, *Chem. Eur. J.* **2012**, *18*, 12227 – 12231; c) S. Ganta, H. Devalapally, A. Shahiwala, M. Amiji, *J. Controlled Release* **2008**, *126*, 187 – 204.
[22] C. Sanson, C. Schatz, J.-F. L. Meins, A. Soum, J. Thevenot, E. Garanger, S. Lecommandoux, *J. Controlled Release* **2010**, *147*, 428 – 435.
[23] Y. L. Li, L. Zhu, Z. Liu, R. Cheng, F. Meng, J. H. Cui, S. J. Ji, Z. Zhong, *Angew. Chem.* **2009**, *121*, 10098 – 10102; *Angew. Chem. Int. Ed.* **2009**, *48*, 9914 – 9918.

